Applicability of Heavy Ion Beam Probing for Stellarator W7-X

S. Perfilov, A. Melnikov, L. Krupnik [1], H.J. Hartfuss[2]

RRC "Kurchatov Institute", Moscow Russia, [1] NNC "KhIPT", Kharkov, Ukraine,
[2] IPP Max-Plank Institute, Greifswald, Germany

Abstract. The feasibility study for HIBP on the stellarator W7-X was done to provide the measurements of the radial profiles of plasma potential, density and their fluctuations. Calculations of probing Tl^+ beam trajectories were done for the various W7-X magnetic configurations with B_0 = 2.5 T. They show that satisfactory access is possible for K11-N11 port combinations. The trajectory optimisation aiming for the maximal plasma observation was done for chosen port combination.

Kay words: plasma potential, probing beam, diagnostic, detector, analyzer

1. Introduction

a) Basic Principles. Heavy Ion Beam Probe (HIBP) is an effective method to measure the poloidal profile of the potential and thus that of the radial electric field in the core of hot magnetized plasmas [1]. When the beam of high-energy single charged ions passes through the plasma, some of the beam ions ionize, predominantly by the electrons. The ionization takes place along the full path of the beam in the plasma. Because of their higher charge state, the secondary ions deviate from the primary beam and form a broad fan of ions leaving the plasma (Fig. 1)

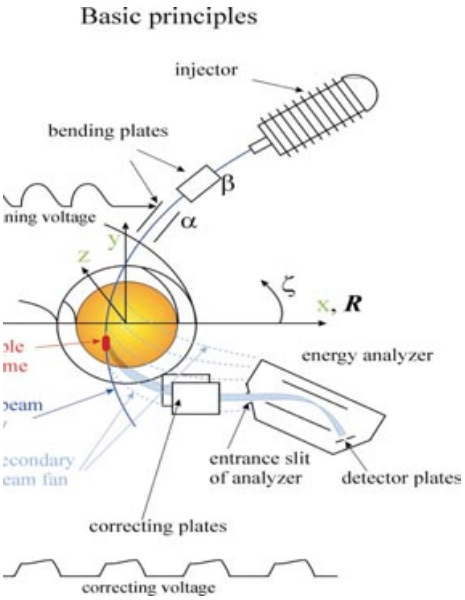

The secondary ions that enter the detector aperture, originate from a small part of the primary beam in the plasma, called the sample volume, which has typical dimensions of (0.5–1) cm^3. The energy difference between the secondary ions leaving the plasma and the primary ions is equal to the electric potential **φ**, at the sample volume. The intensity of the secondary beam reflects the electron density, n_e, in the sample volume. The toroidal velocity of the secondary beam in the detector reflects the poloidal component of magnetic vector potential (poloidal magnetic field or plasma current density).

Redirecting the probing beam with electrostatic sweep plates can rapidly change the position of the sample volume. The position of the sample volume can also be changed shot to shot by changing the energy of the primary particles.
HIBP has a continuous character of the signal, which provides a high temporal resolution, limited by the acquisition electronics.

Fig.1

b) Objectives of the W-7X HIBP project. The idea of the W-7X HIBP project is to provide the plasma potential measurements in the reasonably wide plasma area, which can give various contributions for the W-7X scientific program. The main emphasis is the radial profile of the plasma electric potential. With the measurements of plasma electric potential (mean profiles and fluctuations) HIBP can contribute to the physical understanding of edge (H-

mode) and Internal transport barriers (ITB). Density profile can be reconstructed from the secondary beam intensity profile.

c) W-7X features (difficulties for HIBP). W-7X is not a simple case for HIBP implementation. The relatively low B_{tor} could give a chance of a "low" beam energy needed for the probing. The machine design with large toroidal coils and the high level of the stray magnetic field claims to have rather "long" trajectories located far outside the plasma area as well. That needs the beam transfer units, the beamlines for the primary and the secondary beams adjustment and control.

3D nature of the W7-X magnetic field leads to sufficiently non planar (3D) structure of the beam trajectories. The 2 MeV accelerator is already taken for W-7X HIBP, so the beam energy is limited. The port combination (K11 +N11) was already chosen at the previous stage. The port design brings the geometric limitations for the beam trajectories location. The divertor assembly brings the additional limitation for the trajectories.

2. 3D trajectory calculations. The trajectory calculation code solves the 3D motion equation for the probing particle

$$m\frac{\partial \vec{v}}{\partial t} = qe\vec{E} + qe[\vec{v} \times \vec{B}] \quad (1),$$ where

B - full magnetic field of the device, E – ion energy. The trajectory calculations were done neglecting the plasma electric field. For the W-7X the Tl^+ beam was chosen, m = 205. It was taken the standard HIBP scheme with the basic secondary ionization reaction, producing the secondary ions: $Tl^+ + e = Tl^{++} + 2e$ (2).
So, for the primary beam $\boldsymbol{q}$ = 1, for the secondary particles $\boldsymbol{q}$ = 2. The primary trajectories were originated in the Injection point, located far outside the ports. The secondary trajectories were started from the primary one in the plasma area. They are passed till the Detection point, located far outside the output port. This point may be considered as an entrance slit of the energy analyzer.

a) Magnetic field model. Trajectory calculations were made for the standard W-7X configurations. The vacuum magnetic field was used for this stage of the calculations with B_0 = 2.5T. The 3D structure of the magnetic field was calculated by W-7X magnetic field calculation code (Gourdon code). The spatial grid has a step of 10 cm, the angular step was 1 deg. For the more dense grid the smaller steps were chosen: 5 cm and 0.5deg. The procedure of the interpolation was used for the calculation magnetic field components in the area of calculations. The components of magnetic field were found as a composition of the fields generated by each filament, which were calculated by Biot-Savart law. The filaments positions and currents were taken for the standard configuration [2].

b) Control electric field model. The electric field, generated by the each pair of control (bending) parallel plates is simulated separately. For each pair the full Laplace equation is solved with the finite element method. That means, we don't distinguish the control region and the fringe regions. The electric field is calculated everywhere with the same manner. The calculation shows that the electric potential is less than 10^{-6} of its source (plates) value in a distance a few times larger than plates size). Out of this area the electric potential was neglected. The kinetic energy conservation is verified after the particle leaves the E-field calculation area, within the accuracy better than 10^{-6}.

There were two pairs of the plates modeled for the primary beam control in toroidal and poloidal directions. Both are located outside the machine port.

c) Preliminary calculations.
The verification of the trajectories with the one obtained at the previous stage was done as the initial step of the work**.** The lower port is used for the initial beam injection**.**

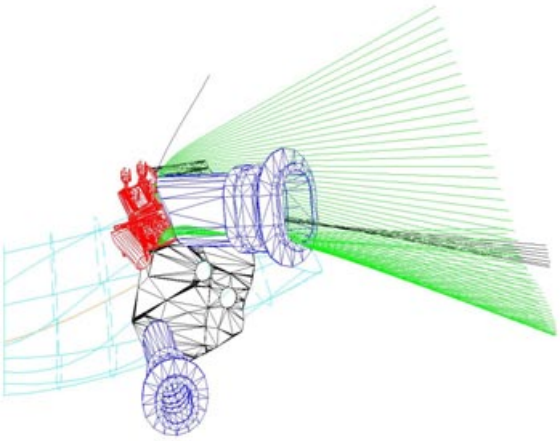

Fig 3. In black - the secondaries for the previous calculations (Courtesy of Dr.U. Neuner). In green – the full secondary fan for the same energy and the initial ……. position.

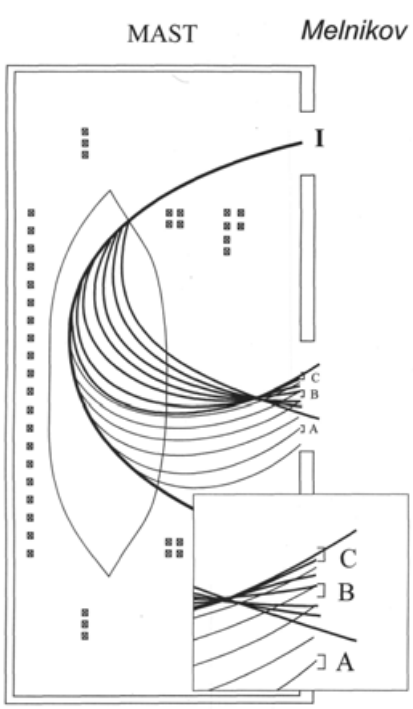

Fig. 2

d) Secondary fan structure. The general scheme of the secondary fan structure is shown in Fig.2 by example of MAST tokamak [3]. The primary trajectory (fat curve) starts in injector port of the vacuum chamber. The secondary fan consists of two parts. The quasi-parallel fan (thin solid curves) covers the detector port from up to down when the birth point moves forward with the primary probing particle. This is the conventional case **'A'.** Some of secondaries intersects in the focus point, because the toroidal field works as the magnetic lens. If detector is located behind the focus, the intersected fan covers the port in opposite direction from down to up when the birth point moves forward with the primary particle. This is the unusual case '**B'**. If detector is located before the focus we get the case **'A'** again. The most general case is the combination of both cases. Two areas can be united if we put the detector in the position **'C'**. Particles ionized in different sample volumes on the same primary trajectories (case A+B) may came to detector with different toroidal deflections. Therefore, the natural way to separate them is to vary the initial toroidal angle. For the case C we are not able to separate two parts of the united sample volume. We have to agree with comparatively poor space resolution, about 10 cm or more.
In Fig. 3 one may see the important features of the secondary fan for the W7-X: 1) it is close to be planar, but not exactly planar,.2) it has U shape in the cross-section. The latter means that not the single one but two trajectories born in different region in plasma may come to the detector simultaneously.

3. The scheme optimized to prevent the intersection between probing trajectories and divertor assembly.

a) **The optimal probing scheme** The probing scheme was found to get the maximal extent of the observation area in plasma and not to disturb the divertor assembly. Fig.4.

b) **Radial reference (B_0=2.5T; E=2MeV)** Fig.5. presents the location of the sample volume for optimal scheme.

.

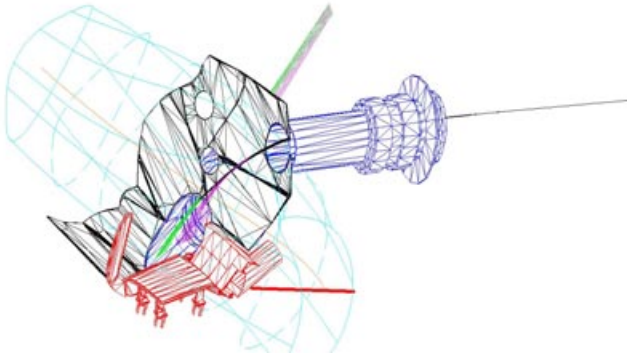

.

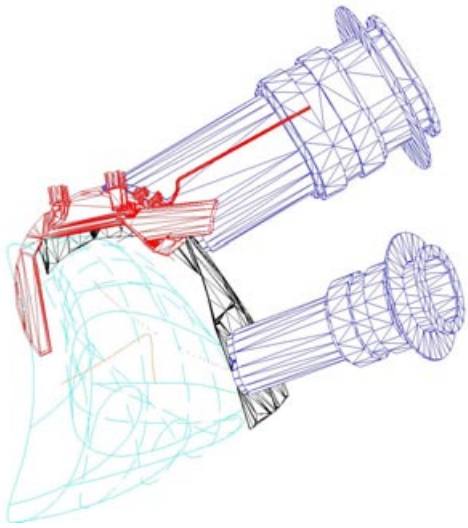

Fig.4. The black line – primary trajectory in the (A11) port, green – secondaties type A, magenda – type B ones.

Fig.5. Orange line – plasma axis; blue – plasma column. Short red pieces – sample volumes on the detector line.

All trajectories are passing the ports A11 and N11 without any loss. The gap between the trajectories and divertor assembly is about the dozen cm.

c. Radial reference for the detector line

One may see the possibility to observe the outer half of plasma radius with type '**B**' trajectories ($0.5<\rho<1.0$). All the trajectories of type '**A**' are born in a very limited radial area ($0.1<\rho<0.15$). The intermediate area ($0.15<\rho<0.5$) belongs to trajectories of type '**C**' with very poor space resolution even for ideal beam of zero width.

To reach the very center of the plasma with optimal probing scheme one need to reduce slightly the toroidal magnetic field up to 2.43MeV. In this case the trajectories of type '**A**' will reach the center.

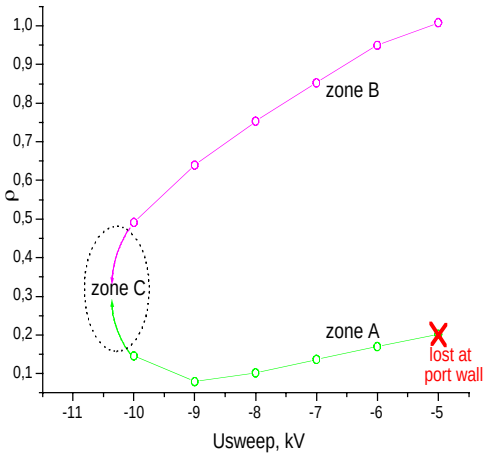

Fig.6. Radial reference versus Usweep (injection angle).

4. The trajectories calculations modelling the real beam dimensions.

The sample volume splitting and existance of the 'C' zone cause the substantional rise of the sample volume (deterioration of the spatial resolution).

For W7-X thick beam calculations we have fixed 2cm beam width. Thick beam is modelled with a set of 100 beam filaments. The Gaussian beam current distribution was modelled. The sample volumes for zone "B" and the corresponding radii are presented in Figure 7. It is assumed that the secondaries from zone "A" were killed by the collimation.

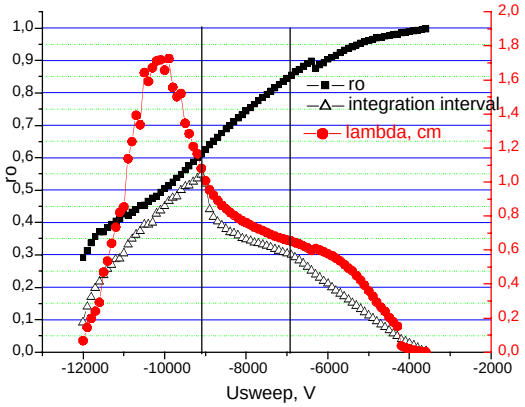

Fig.7 "Thick beam" calculation results

The open triangles – the integration interval (radial length of the sample volume). The sqaures – the radius of the centre of mass for the sample volume. The red circles presents the modelled beam current in the analyser (case of the uniformed plasma density).

In the interval from – 7 000 V to approximately - 4 000 V of Usweep ($0.85 < \rho < 1.0$) some part of the secondary beam, reaching the detector, was born outside the plasma border. That is the reason of the decrease of the red curve when sample volume moves to the plasma border (Usweep tends to –4 000 V).

In the interval from – 9 000 V to approximately - 7 000 V of Usweep ($0.6 < \rho < 0.85$) there are no any beam losses. In principle , the good area for the measurements. One can see that the integration interval is $0.3<\Delta\rho<0.5$ for this area. Such space resolution is extremely poor.

In the interval from –12 000 V to approximately - 9 000 V of Usweep ($0.3 < \rho < 0.6$) there are some losses of the secondaries born at the several filaments. It starts from peripheral filaments at Usweep = –12 000 V. At the final point Usweep = –12 000 V all of them are missed.

We can conclude that the integration interval is unaffordably high for this probing scheme.

5. The study aiming to improve the spatial resolution for the standard configuration.

We discussed the features of the optimized probing scheme in previous chapter. We note rather limited observation area for this scheme and rather poor spatial resolution (see Fig 7).

To improve the spatial resolution the optimal scheme was modified. The main idea of the trajectories modification was to separate as much as possible the C-zone from the area of measurements. The possible mean was found to vary the distance between the Injection and Detection points. One should take care about the geometrical limitations due to port size and the divertor assembly location. It was taken the realistic beam diameter d = 10 mm for the modeling.

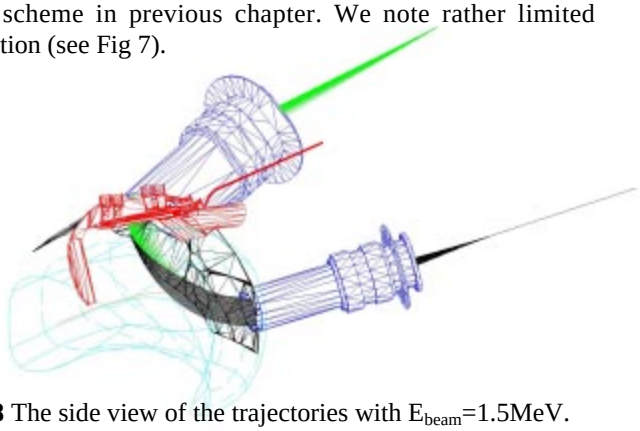

Fig.8 The side view of the trajectories with E_{beam}=1.5MeV.

a. the use of the A-type trajectories

To observe the detector line formed with A type of the trajectories the Injection point was shifted up. To let the trajectories pass throw the ports we have to reduce the beam energy to E_{beam} = 1.5 MeV.
The probing scheme parameters are: Xinj = 422.6 cm, **Yinj = 129.2 cm**, Z inj = 223 cm, Xdet = 232.7 cm, Ydet = 281.7 cm, Z det is not fixed. The trajectories do not intersect the divertor assembly.
Note that the total radial observation interval becomes shorter (compare to Fig. 7).

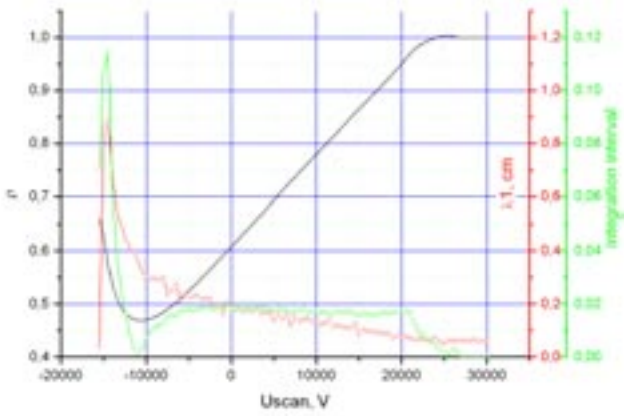

Fig.9. "Thick beam" calculation results
In green – the integration interval (radial length of the sample volume as a fraction of $a_{seperatrix}$) for d_{beam} = 10 mm. In black – the radius of the centre of mass for the sample volume. In red - the length of the sample volume along the primary trajectory, λ. It is shown the averaged value over all the beam filaments.

The C-zone (-15 000 V < Usweep < -12 000 V) manifests itself by drastic increase of λ and the integration interval. In the interval from – 10 000 V to approximately + 20 000 V of Usweep (0.48 < ρ <0.95), which can be used for the measurements, there are no any beam losses. In principle, it is the good area for the measurements. One can see that the integration interval is 0.01 < Δρ < 0.02. This is quite small value in comparison with the case described in Fig 13, which is 0.3 < Δρ < 0.5 for 0.6 < ρ <0.85. The disadvantage of the discussed case is rather wide interval of the sweeping voltage.

Finally, obtained spatial resolution is reasonably acceptable and the observation area is extended. It still remains too short.

Note that some part of the secondary beam, reaching the detector, was born outside the plasma border. That is the reason of the decrease of the green curve when sample volume moves to the plasma border (20 000 V < Usweep < 30 000 V).

b. the use of the B-type trajectories

To observe the detector line formed with B type of the trajectories the Detection point was shifted up. There are no necessity to reduce the beam energy to let the trajectories pass throw the ports in this case. So we keep the maximal E_{beam} = 2.0 MeV.

The probing scheme parameters are:
Xinj = 422.6 cm, Yinj = 124.2 cm, Z inj = 223 cm
Xdet = 232.7 cm, **Ydet = 230 cm**, Z det is not fixed

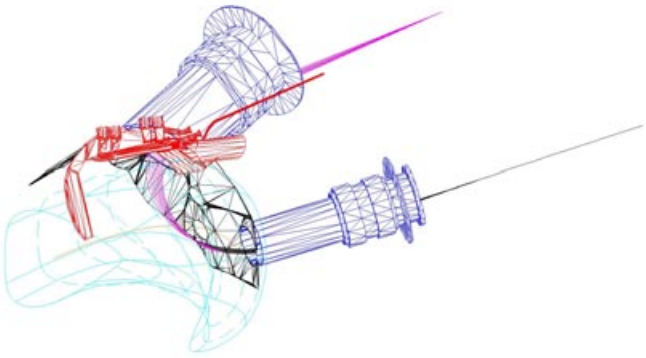

Fig 10. The side view of the trajectories with **E_{beam} = 2.0 MeV**.

The trajectories do not intersect the divertor assembly.
Note that the total radial observation interval becomes shorter (compare to Fig. 7).

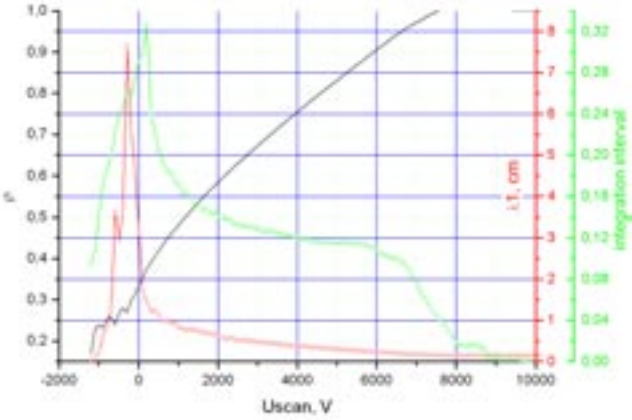

Fig.11. "Thick beam" calculation results
In green – the integration interval (radial length of the sample volume as a fraction of $a_{seperatrix}$) d_{beam} = 10 mm. In black – the radius of the centre of mass for the sample volume. In red - the length of the sample volume along the primary trajectory, λ. It is shown the averaged value over all the beam filaments.

The C-zone is seen clearly in the interval (-1 500 V < Usweep < +1 500 V). In the interval from +1 500 V to approximately + 7 500 V of Usweep (0.45 < ρ <0.95), which can be used for the measurements, there are no any beam losses. Again, it is the good area for the measurements. One can see that the integration interval is 0.12 < Δρ < 0.16. This is quite large value in comparison with the case described in Fig. 17, unless smaller than the case, described in Fig. 13, which is 0.3 < Δρ < 0.5 for 0.6 < ρ <0.85. The advantage of the discussed case is rather narrow interval of the sweeping voltage.

Finally, obtained spatial resolution looks to be marginally acceptable. The observation area is the same as for A-type trajectories.

Similar to the A-type trajectories, some part of the secondary beam, reaching the detector, was born outside the plasma border. That is the reason of the decrease of the green curve when sample volume moves to the plasma border (6 000 V < Usweep < 9 000 V).

6. Beam attenuation estimations.

The beam attenuation was calculated with the following equations. For primary beam:

$R_{primary} = \exp(-\oint_{primary} n_e \sigma_{eff}^{1,2} dl)$, where $\sigma_{\text{eff}}^{1,2}$ - effective cross-section for electron impact ionization

$\sigma_{\text{eff}}^{1,2} = <\sigma^{1,2} V_e> / V_{\text{beam}}$. For the secondary beam $R_{\text{secondary}} = \exp(-\int_{\text{secondary}} n_e \sigma_{\text{eff}}^{2,3} dl)$, where $\sigma_{\text{eff}}^{2,3} \approx \frac{\sigma_{\text{eff}}^{1,2}}{3}$ due to the Lotz formula.

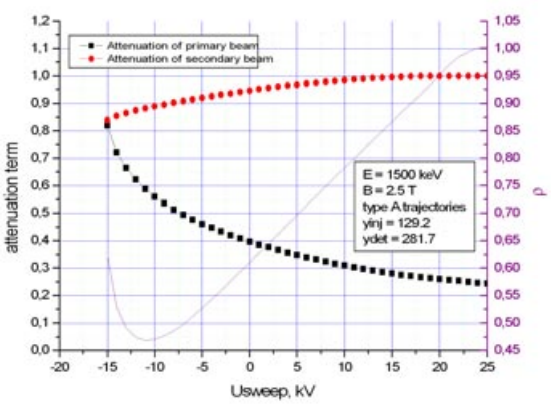

Fig.12. Results of the calculations for the A-type trajectories.

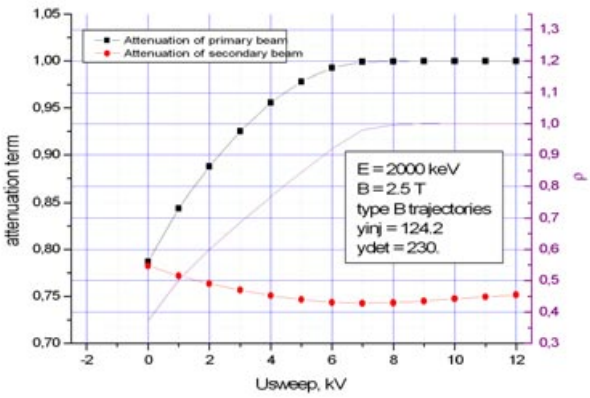

Fig.13. Results of the calculations for the B-type trajectories.

7. Conclusions:

1. The optimized probing scheme for K11-N11 port combination was found. 2.This scheme allows us to avoid intersection between beam trajectory and divertor plates assembly. 3. Radial range for sample volume for {2.5 T, 2 MeV} is 0.08 < ρ < 1.0. 4.The sample volume splitting takes place for the analyzed port combination. To select the desired trajectories, the secondary beam collimation is needed. 5. The real observable area is only 0.45 < ρ < 0.95. There was found a possibility to get quite good spatial resolution 0.012 < Δρ < 0.015 for 1 cm beam diameter 6. The beam attenuation looks to be acceptable for the measurements in the continuous beam current.

Acknowledgements.

We appreciate the collaboration with Dr Harmeyer, Dr Kisslinger and Dr Neuner. This work has been supported by INTAS Grant No2001-2056 and RFBR Grant 05-02-17016.

Reference:

[1] IEEE Transaction on the Plasma Science, August 1994. Special Issue on HIBP.

[2] T. Andreeva, "Vacuum Magnetic Configurations of Wendelstein 7-X." Preprint IPP III/270 May 2002.

[3] A. Melnikov and S. Perfilov, Rev. Sci. Instrum, Vol.70, No2, P.1402, 1999.